



Comparison among Unstructured TVD, ENO and UNO Schemes in Three-Dimensions

Edisson Sávio de Góes Maciel¹, Cláudia Regina de Andrade²

¹Instituto Tecnológico de Aeronáutica (ITA) – Rua Santa Clara, 245 – Caixa Postal: 2029 – 12.243-970 – São José dos Campos – SP – Brazil

²Instituto Tecnológico de Aeronáutica (ITA) – Praça Mal. do Ar Eduardo Gomes, 50 – 12.228-900 – São José dos Campos – SP – Brazil

Abstract This study focuses on unstructured TVD, ENO and UNO schemes applied to solve the Euler equations in three-dimensions. They are implemented on a finite volume context and cell centered data base. The algorithms of Yee, Warming and Harten 1982; Harten; Yee and Kutler; Yee Warming and Harten 1985; Yee; Yee and Harten; Harten and Osher; Hughson and Beran; Yang; and Yang and Hsu are implemented to solve such system of equations in three-dimensions. All schemes are flux difference splitting and good resolution is expected. This study deals with calorically perfect gas model and in so on the cold gas formulation is employed. Two problems are studied, namely: the transonic convergent-divergent symmetrical nozzle, and the supersonic ramp. A spatially variable time step is implemented to accelerate the convergence process. The results highlights the excellent performance of the Harten scheme in the nozzle problem, yielding an excellent pressure distribution at the nozzle wall, whereas the Yee and Harten scheme yields accurate value to the angle of the oblique shock wave and the best wall pressure distribution in the ramp problem.

Keywords TVD, ENO, UNO, Three-Dimensions

1. Introduction

High resolution upwind schemes have been developed since 1959, aiming to improve the generated solution quality, yielding more accurate solutions and more robust codes. The high resolution upwind schemes can be of flux vector splitting type or flux difference splitting type. In the former case, more robust algorithms are yielded, while in the latter case, more accuracy is obtained. Several studies were performed involving high resolution TVD algorithms in the international literature, as for example:

The scheme of [1] is a flux difference splitting one, which utilizes the concept of TVD (“Total Variation Diminishing”). It utilizes the concept of a modified inviscid flux vector to calculate the numerical fluxes. It utilizes artificial compressibility terms to take into account compressibility effects. The second order of accuracy is obtained with an appropriate definition of the modified numerical flux. The scheme satisfies a proper entropy inequality to ensure that the limit solution will have only physically relevant discontinuities. This scheme is second-order accurate in space and time. The time integration is accomplished by a Runge-Kutta procedure in this work.

The work of [2] defined a class of new explicit second-order accurate finite difference schemes, for the computation of weak solutions of hyperbolic conservation laws. The highly non-linear schemes were obtained by applying a non-oscillatory first-order accurate scheme to an appropriately modified flux function. The so-derived second-order accurate schemes achieve high resolution while preserving the robustness of the original non-oscillatory first-order accurate scheme. These schemes are called TVD (“Total Variation Diminishing”) ones and yield physically relevant solutions by the use of an entropy condition. Our implementation of the [2]



scheme is accomplished on a finite volume context. This scheme is second-order accurate in space. The time integration is accomplished by a Runge-Kutta method of two stages.

The work of [3] emphasized that a one-parameter family of explicit and implicit second order accurate, entropy satisfying, total variation diminishing (TVD) schemes had been developed by [2]. These schemes had the property of not generating spurious oscillations for one-dimensional non-linear scalar hyperbolic conservation laws and constant coefficient hyperbolic systems. Application of these methods to one- and two-dimensional fluid flows containing shocks (in Cartesian coordinates) yielded highly accurate non-oscillatory numerical solutions. The goal of the work of [3] was to extend these methods to the multidimensional Euler equations in generalized coordinate systems. The scheme is second order accurate in space and time. The time integration is accomplished by a Runge-Kutta method of two stages, second order accurate.

In their work, [4] applied a new implicit unconditionally stable high resolution TVD scheme to steady state calculations. It was a member of a one-parameter family of explicit and implicit second order accurate schemes developed by [2] for the computation of weak solutions of one-dimensional hyperbolic conservation laws. The scheme was guaranteed not to generate spurious oscillations for a nonlinear scalar equation and a constant coefficient system. Numerical experiments have shown that the scheme not only had a fairly rapid convergence rate, but also generated a highly resolved approximation to the steady state solution. A detailed implementation of the implicit scheme for the one- and two-dimensional compressible inviscid equations of gas dynamics was presented. Some numerical experiments of one- and two-dimensional fluid flows containing shocks demonstrated the efficiency and accuracy of the new scheme.

In her work, [5] reformulated a one-parameter family of second-order explicit and implicit total variation diminishing (TVD) schemes so that a simpler and wider group of limiters was included. The resulting scheme can be viewed as a symmetrical algorithm with a variety of numerical dissipation terms that were designed for weak solutions of hyperbolic problems. This was a generalization of the works of Roe and Davis to a wider class of symmetric schemes other than Lax-Wendroff. The main properties of this class of schemes were that they could be implicit, and, when steady-state calculations were sought, the numerical solution was independent of the time step. Numerical experiments with two-dimensional unsteady and steady-state airfoil calculations have shown that the proposed symmetric TVD schemes were quite robust and accurate. In the present study, only the results with the Minmod limiter, Eq. (44), are presented.

In their work, [6] considered that Harten's method of constructing high resolution TVD schemes involves starting with a first-order TVD scheme and applying it to a modified flux. The modified flux is chosen so that the scheme is second-order at regions of smoothness and first-order at points of extrema. This technique is sometimes referred to as the modified flux approach. [6] extended a TVD scheme (via the modified flux approach) to generalized coordinate systems and discussed the various solution strategies for the implicit TVD schemes for more efficient two-dimensional steady-state applications. The TVD scheme was initially an implicit TVD one developed to solve a two-dimensional gas-dynamic problem in Cartesian coordinate.

Considering the axisymmetric configurations, [7] presented an explicit, second order accurate, total variation diminishing (TVD) scheme applied to the Euler equations in axisymmetric form to study hypersonic blunt-body flows. The modified flux function approach of [2], with modification by [8], for two-dimensional flows is extended to treat axisymmetric flows. The scheme was presented on a finite difference context, but in our implementation, the scheme is written on a finite volume context. Roe's averaging for a perfect gas was used to assess the eigenvalues and eigenvectors at cell interfaces, because it has the computational advantage of resolving stationary discontinuities. An entropy condition is implemented to assure relevant physical solutions. Linear and non-linear limiters (g 's functions) assure second order accuracy as well control the amount of numerical dissipation added to the flow equations.

A new class of uniformly high order accurate essentially nonoscillatory (ENO) schemes have been developed by [9-12]. They presented a hierarchy of uniformly high order accurate schemes that generalize [13]'s scheme, its second order accurate MUSCL extension ([14-15]), and the total variation diminishing (TVD) scheme ([2]) to arbitrary order of accuracy. In contrast to the earlier second order TVD schemes which drop to first order accuracy at local extrema and maintain second order accuracy in smooth regions, the new ENO schemes are uniformly high order accurate throughout, even at critical points. The ENO schemes use a reconstruction



algorithm that is derived from a new interpolation technique that when applied to piecewise smooth data gives high order accuracy whenever the function is smooth but avoids a Gibbs phenomenon at discontinuities. An adaptive stencil of grid points is used; therefore, the resulting schemes are highly nonlinear even in the scalar case. Some schemes constructed in this way were:

Considering ENO schemes, [9] presented a hierarchy of uniformly high order accurate schemes that generalize [13] scheme, and its second order accurate extension of monotonic upstream schemes for conservation laws (MUSCL) ([14-15]) and total variation diminishing (TVD) schemes ([2] and [16]) to arbitrary order of accuracy. In her work, [17] emphasized a two time-level third order finite-difference shock-capturing schemes based on applying the characteristic flux difference splitting to a modified flux that may have high-order accuracy and either monotonicity preserving or essentially nonoscillatory (ENO) property have been developed for the Euler equations of gas dynamics. Two ways to achieve high-order accuracy were described in his work. One was based on upstream interpolation using Lagrange’s formula with Van Leer’s smoothness monitor. The other was based on ENO interpolation using reconstruction via primitive function approaches. For multidimensional problems, dimensional splitting was adopted for explicit schemes, and standard alternating direction implicit approximate factorization procedure was used for implicit schemes. He gave some examples to illustrate the performance of the proposed ENO schemes.

In their work, [18] developed a high-resolution explicit finite difference nonoscillatory shock-capturing schemes based on Harten’s essentially nonoscillatory interpolation using reconstruction via primitive function approach with $N = 3$ for simulating unsteady compressible flow. The extension to nonlinear system was done using Roe’s method, which permitted the use of different scalar schemes for different characteristic fields. For multidimensional problems, a Runge-Kutta scheme was adopted. Numerical simulations of unsteady shock diffraction by an elliptic cylinder and shock wave propagating through a convergent-divergent nozzle were studied in their original paper.

In the current paper, the Euler equations in three-dimensions are solved by the use of TVD, ENO and UNO schemes, second and third order accurate. The following ten flux difference splitting algorithms are employed: [1-7], on a TVD approach and [9, 17], on an ENO approach, and finally [18], on a UNO approach. A finite volume formulation is employed on conservative and unstructured contexts. The time discretization employs a Runge-Kutta method of two steps. All ten algorithms are applied to the solution of two problems: the transonic convergent-divergent nozzle, and the supersonic ramp. All schemes are accelerated to the steady state solution using a spatially variable time step procedure, which has proved excellent characteristics of convergence [19-20]. The results have demonstrated that the best result of the wall pressure distribution in the nozzle case is due to [2] and the best wall pressure distribution and shock angle in the ramp case is due to [6].

2. Euler Equations

The fluid movement is described by the Euler equations, which express the conservation of mass, of linear momentum and of energy to an inviscid medium, heat non-conductor and compressible, in the absence of external forces. In integral and conservative forms, these equations can be given by:

$$\frac{\partial}{\partial t} \int_V Q dV + \iint_S [(E_e)_x n_x + (F_e)_y n_y + (G_e)_z n_z] dS = 0, \tag{1}$$

with Q written to a Cartesian system, V is the cell volume, n_x , n_y and n_z are the components of the normal unity vector to the flux face, S is the flux area, and E_e , F_e and G_e are the convective flux vector components. The Q , E_e , F_e and G_e vectors are represented by:

$$Q = \begin{Bmatrix} \rho \\ \rho u \\ \rho v \\ \rho w \\ e \end{Bmatrix}, \quad E_e = \begin{Bmatrix} \rho u \\ \rho u^2 + p \\ \rho uv \\ \rho uw \\ (e + p)u \end{Bmatrix}, \quad F_e = \begin{Bmatrix} \rho v \\ \rho uv \\ \rho v^2 + p \\ \rho vw \\ (e + p)v \end{Bmatrix} \quad \text{and} \quad G_e = \begin{Bmatrix} \rho w \\ \rho uw \\ \rho vw \\ \rho w^2 + p \\ (e + p)w \end{Bmatrix}, \tag{2}$$



being ρ the fluid density; u , v and w the Cartesian components of the velocity vector in the x , y and z directions, respectively; e the total energy; and p the static pressure of the fluid medium.

In the studied problems, the Euler equations were nondimensionalized in relation to the freestream density, ρ_∞ , and in relation to the freestream speed of sound, a_∞ . Hence, the density is nondimensionalized in relation to ρ_∞ ; the u , v and w velocity components are nondimensionalized in relation to a_∞ ; and the pressure and the total energy are nondimensionalized in relation to the product $\rho_\infty(a_\infty)^2$. The matrix system of the Euler equations is closed with the state equation $p = (\gamma - 1)[e - 0.5\rho(u^2 + v^2 + w^2)]$, assuming the ideal gas hypothesis. The total enthalpy is determined by $H = (e + p)/\rho$.

Equation (1) describes a relation in which the time rate of variation of the Q state vector, inside a V volume, is balanced by the net convective flux which crosses the S boundary surface. The calculation domain is divided in a great number of tetrahedral cells and the Eq. (1) is applied to each cell.

3. Yee, Warming and Harten (1982) TVD Algorithm

The algorithm of [1], second order accurate in space, is specified by the determination of the numerical flux vector at “I” interface.

Following a finite volume formalism, which is equivalent to a generalized coordinate system, the right and left cell volumes, as well the interface volume, necessary to a coordinate change, are defined by:

$$V_R = V_{ne}, \quad V_L = V_i \quad \text{and} \quad V_1 = 0.5(V_R + V_L), \quad (3)$$

where “R” and “L” represent right and left states, respectively, and “ne” represent a neighbor volume to the “i” volume. In this work, it was adopted that “L” is associated to properties of a given “i” volume and “R” is associated to properties of the “ne” neighbor volume. The cell volume, the surface areas, the normal unity vector components are defined in [21] for each cell. The description of the computational cell and its nodes, flux interfaces and neighbors are also shown in [21].

The metric terms to this generalized coordinate system are defined as:

$$h_x = S_x^1/V_1, \quad h_y = S_y^1/V_1, \quad h_z = S_z^1/V_1 \quad \text{and} \quad h_n = S^1/V_1, \quad (4)$$

where S_x^1 , S_y^1 and S_z^1 are the flux surfaces areas.

The properties calculated at the flux interface are obtained by arithmetical average or by Roe average. In the present work, the Roe average was used:

$$\rho_1 = \sqrt{\rho_R \rho_L}, \quad u_1 = \frac{u_R \sqrt{\rho_R} + u_L \sqrt{\rho_L}}{\sqrt{\rho_R} + \sqrt{\rho_L}}, \quad v_1 = \frac{v_R \sqrt{\rho_R} + v_L \sqrt{\rho_L}}{\sqrt{\rho_R} + \sqrt{\rho_L}}, \quad w_1 = \frac{w_R \sqrt{\rho_R} + w_L \sqrt{\rho_L}}{\sqrt{\rho_R} + \sqrt{\rho_L}}; \quad (5)$$

$$H_1 = \frac{H_R \sqrt{\rho_R} + H_L \sqrt{\rho_L}}{\sqrt{\rho_R} + \sqrt{\rho_L}} \quad \text{and} \quad a_1 = \sqrt{(\gamma - 1)[H_1 - 0.5(u_1^2 + v_1^2 + w_1^2)]}, \quad (6)$$

where a_1 is the speed of sound at the flux interface. The eigenvalues of the Euler equations, in the normal direction to the flux face, to the convective flux are given by:

$$q_{\text{normal}} = u_1 h_x + v_1 h_y + w_1 h_z, \quad \lambda_1 = q_{\text{normal}} - a_1 h_n, \quad \lambda_2 = \lambda_3 = \lambda_4 = q_{\text{normal}} \quad \text{and} \\ \lambda_5 = q_{\text{normal}} + a_1 h_n. \quad (7)$$

The jumps of the conserved variables, necessary to the construction of the [1] dissipation function, are given by:

$$\Delta e = V_1(e_R - e_L), \quad \Delta \rho = V_1(\rho_R - \rho_L), \quad \Delta(\rho u) = V_1[(\rho u)_R - (\rho u)_L], \quad \Delta(\rho v) = V_1[(\rho v)_R - (\rho v)_L]; \quad (8)$$

$$\Delta(\rho w) = V_1[(\rho w)_R - (\rho w)_L]; \quad (9)$$

The α vectors to the “I” interface are calculated by the following matrix-vector product:

$$\{\alpha_i^m\} = [R^{-1}]_I \{\Delta_{\text{int}} Q\}, \quad (10)$$

with: $\Delta_{\text{int}} = (\cdot)_{ne} - (\cdot)_i$ and $[R^{-1}]$ defined according to [22].



The dissipation function of [1] uses the right-eigenvector matrix of the normal to the flux face Jacobian matrix in generalized coordinates, [R]. This matrix is also defined in [22].

Two options to the ψ_m entropy function, responsible to guarantee that only relevant physical solutions are to be considered, are implemented aiming an entropy satisfying algorithm:

$$v_m = \Delta t \lambda_m = Z_m \text{ and } \psi_m = Z_m^2 + 0.25; \tag{11}$$

Or:

$$\psi_m = \begin{cases} |Z_m|, & \text{if } |Z_m| \geq \delta_f \\ 0.5(Z_m^2 + \delta_f^2) / \delta_f, & \text{if } |Z_m| < \delta_f \end{cases}, \tag{12}$$

where “m” varies from 1 to 5 (three-dimensional space) and δ_f assuming values between 0.1 and 0.5, being 0.2 the recommended value by [1]. In the present studies, Eq. (11) was used to perform the numerical experiments.

The \tilde{g} function at the “I” interface is defined by:

$$\tilde{g}_i^m = 0.5(\psi_m - Z_m^2)\alpha_i^m. \tag{13}$$

The g numerical flux function, which is a limited function to avoid the formation of new extremes in the solution and is responsible to the second order accuracy of the scheme, is given by:

$$g_i^m = \text{signal}_m \times \text{MAX}(0.0; \text{MIN}(\tilde{g}_i^m, \tilde{g}_{i-1}^m \times \text{signal}_m)), \tag{14}$$

Where signal_m is equal to 1.0 if $\tilde{g}_i^m \geq 0.0$ and -1.0 otherwise.

The θ term, responsible to the artificial compressibility, as referred in the CFD community, which enhances the resolution of the scheme at discontinuities, is defined as follows:

$$\theta_i^m = \begin{cases} |\alpha_i^m - \alpha_{i-1}^m| / (|\alpha_i^m| + |\alpha_{i-1}^m|), & \text{if } |\alpha_i^m| + |\alpha_{i-1}^m| \neq 0.0 \\ 0.0, & \text{if } |\alpha_i^m| + |\alpha_{i-1}^m| = 0.0 \end{cases}; \tag{15}$$

The β vector at the “I” interface, which introduces the artificial compression term in the algorithm, is defined by the following expression:

$$\beta_m = 1.0 + \omega_m \text{MAX}(\theta_i^m, \theta_{i+1}^m), \tag{16}$$

where ω_m assumes the following values: $\omega_1 = 0.25$ (non-linear field), $\omega_2 = \omega_3 = \omega_4 = 1.0$ (linear field) and $\omega_5 = 0.25$ (non-linear field).

The numerical characteristic speed, ϕ_m , at the “I” interface, which is responsible to transport the numerical information associated to the g numerical flux function, is defined by:

$$\phi_m = \begin{cases} (g_{i+1}^m - g_i^m) / \alpha^m, & \text{if } \alpha^m \neq 0.0 \\ 0.0, & \text{if } \alpha^m = 0.0 \end{cases}. \tag{17}$$

The entropy function is redefined considering ϕ_m and β_m : $Z_m = v_m + \beta_m \phi_m$, and ψ_m is recalculated according to Eq. (11) or to Eq. (12). Finally, the [1] dissipation function, to second order accuracy in space, is constructed by the following matrix-vector product:

$$\{D_{YWH82}\}_1 = [R]_1 \left\{ \frac{(\beta(g_i + g_{i+1}) - \psi\alpha)}{\Delta t_i} \right\}_1. \tag{18}$$

The convective numerical flux vector to the “I” interface is described by:

$$VF_1^{(m)} = (E_1^{(m)}h_x + F_1^{(m)}h_y + G_1^{(m)}h_z)N_1 + 0.5D_{YWH}^{(m)}, \tag{19}$$

with:

$$E_1^{(m)} = 0.5(E_R^{(m)} + E_L^{(m)}), F_1^{(m)} = 0.5(F_R^{(m)} + F_L^{(m)}) \text{ and } G_1^{(m)} = 0.5(G_R^{(m)} + G_L^{(m)}). \tag{20}$$



The time integration is performed by an explicit method, second order accurate, Runge-Kutta type of two stages and can be represented of generalized form by:

$$\begin{aligned} Q_i^{(0)} &= Q_i^{(n)} \\ Q_i^{(k)} &= Q_i^{(0)} - \alpha_k \Delta t_i / V_i \times C(Q_i^{(k-1)}), \\ Q_i^{(n+1)} &= Q_i^{(k)} \end{aligned} \tag{21}$$

with $k = 1, 2$; $\alpha_1 = 1/2$, $\alpha_2 = 1$. The contribution of the convective numerical flux vectors is determined by the C_i vector:

$$C_i^{(m)} = VF_1^{(m)} + VF_2^{(m)} + VF_3^{(m)} + VF_4^{(m)}. \tag{22}$$

4. Harten (1983) TVD Algorithm

The algorithm of [2], second order accurate in space, follows the Eqs. (3) to (10). The next step is the definition of the entropy condition, which is defined by Eq. (11), v_m , and Eq. (12).

The \tilde{g} function at the “I” interface is defined according to Eq. (13) and the g numerical flux function is given by Eq. (14). The numerical characteristic speed ϕ_m at the “I” interface is defined according to Eq. (17).

The entropy function is redefined considering $\phi_m : Z_m = v_m + \phi_m$, and ψ_m is recalculated according to Eq. (12). Finally, the [2] dissipation function, to second order spatial accuracy, is constructed by the following matrix-vector product:

$$\{D_{Harten}\}_1 = [R]_1 \{ (g_i + g_{i+1} - \psi\alpha) / \Delta t_i \}_1. \tag{23}$$

Equations (19), (20) and (22) are used to conclude the numerical flux vector of the [2] scheme and the time integration is performed by the Runge-Kutta method defined by Eq. (21).

5. Yee and Kutler (1985) TVD Algorithm

The algorithm of [3], second order accurate in space, follows Eqs. (3) to (10). The next step consists in determining the θ function. This function is defined in terms of the differences of the gradients of the characteristic variables to take into account discontinuities effects and is responsible to artificial compression:

$$\theta_i^m = \begin{cases} \frac{|\alpha_i^m - \alpha_{i-1}^m|}{\alpha_i^m + \alpha_{i-1}^m}, & \text{if } (\alpha_i^m + \alpha_{i-1}^m) \neq 0.0 \\ 0.0, & \text{if } (\alpha_i^m + \alpha_{i-1}^m) = 0.0 \end{cases}. \tag{24}$$

The κ function at the “I” interface is defined as follows:

$$\kappa_m = 1/8 (1 + \omega_m \text{MAX}(\theta_i^m, \theta_{i+1}^m)), \tag{25}$$

The g numerical flux function is determined by:

$$g_i^m = \text{signal}_m \times \text{MAX}(0.0; \text{MIN}(|\alpha_i^m|, \alpha_{i-1}^m \times \text{signal}_m)), \tag{26}$$

Where signal_m assumes value 1.0 if $\alpha_i^m \geq 0.0$ and -1.0 otherwise. The numerical characteristic speed ϕ_m at the “I” interface is calculated by the following expression:

$$\phi_m = \begin{cases} \kappa_m (g_{i+1}^m - g_i^m) / \alpha^m, & \text{if } \alpha^m \neq 0.0 \\ 0.0, & \text{if } \alpha^m = 0.0 \end{cases}. \tag{27}$$

The ψ_1 entropy function at the “I” interface is defined by:

$$\psi_m = (v_m + \phi_m)^2 + 0.25, \tag{28}$$

with v_m defined according to Eq. (11). Finally, the [3] dissipation function, to second order spatial accuracy, is constructed by the following matrix-vector product:

$$\{D_{Yee/Kutler}\}_1 = [R]_1 \{(\kappa(g_i + g_{i+1}) - \psi\alpha) / \Delta t_i\}_1. \tag{29}$$

Equations (19), (20) and (22) are used to conclude the numerical flux vector of [3] scheme and the time integration is performed by the Runge-Kutta method defined by Eq. (21).

6. Yee, Warming and Harten (1985) TVD Algorithm

The numerical scheme of [4], second order accurate in space, follows Eqs. (3) to (10). The next step is to calculate the numerical flux function, g. The g numerical flux function, which is a limited function to avoid the formation of new extrema in the solution and is responsible to the second order accuracy of the scheme, is given by:

$$g_i^m = \text{signal}_m \times \text{MAX}[0.0; (\sigma_i^m |\alpha_i^m|, \text{signal}_m \times \sigma_{i-1}^m \alpha_{i-1}^m)], \tag{30}$$

Where signal_m is equal to 1.0 if $\alpha_i^m \geq 0.0$ and -1.0 otherwise; $\sigma_1(\lambda_1) = 0.5Q_1(\lambda_1)$; and Q is given by:

$$Q_m(Z_m) = \begin{cases} |Z_m|, & \text{if } |Z_m| \geq \delta_f \\ 0.5(Z_m^2 + \delta_f^2) / \delta_f, & \text{if } |Z_m| < \delta_f \end{cases}, \tag{31}$$

where “m” varies from 1 to 5 (three-dimensional space) and δ_f assumes values between 0.1 and 0.5, being 0.2 the value recommended by [4]. The θ term, responsible to the artificial compression, which enhances the resolution of the scheme at discontinuities like shock waves and contact discontinuities, is defined as:

$$\theta_i^m = \begin{cases} |\alpha_i^m - \alpha_{i-1}^m| / (|\alpha_i^m| + |\alpha_{i-1}^m|), & \text{if } |\alpha_i^m| + |\alpha_{i-1}^m| \neq 0.0; \\ 0.0, & \text{if } |\alpha_i^m| + |\alpha_{i-1}^m| = 0.0. \end{cases} \tag{32}$$

The β parameter at the l interface, which introduces the artificial compression term, is given by:

$$\beta_i = 1.0 + \omega_1 \theta_i^m, \tag{33}$$

in which ω_1 assumes the following values: $\omega_1 = 0.25$ (non-linear field), $\omega_2 = \omega_3 = \omega_4 = 1.0$ (linear field) and $\omega_5 = 0.25$ (non-linear field). The \tilde{g} function is defined by:

$$\tilde{g}_i^m = \beta_i g_i^m. \tag{34}$$

The numerical characteristic speed, ϕ_1 , at the l interface, which is responsible to transport the numerical information associated to the g numerical flux function, or indirectly through \tilde{g} , is defined by:

$$\phi_m = \begin{cases} (\tilde{g}_{i+1}^m - \tilde{g}_i^m) / \alpha^m, & \text{if } \alpha^m \neq 0.0; \\ 0.0, & \text{if } \alpha^m = 0.0. \end{cases} \tag{35}$$

Finally, the dissipation function of [4], to second order of spatial accuracy, is constructed by the following matrix-vector product:

$$\{D_{YWH85}\}_1 = [R]_1 \{(g_i + g_{i+1}) - Q(\lambda + \phi)\alpha\}_1. \tag{36}$$

The convective numerical flux vector to the “l” interface is described by Eqs. (19), (20) and (22) and the time integration is performed by Eq. (21).

7. Yee (1987) TVD Symmetrical Algorithm

The symmetrical algorithm of [5], second order accurate in space, follows Eqs. (3) to (10). The next step is to calculate the entropy function. It is determined by Eq. (12) using the eigenvalues, Eq. (7), of the Euler equations as variables. After that, the Q function is determined. In the present work, five options were implemented. They are:

$$Q(r^-, r^+) = \min \text{mod}(1, r^-) + \min \text{mod}(1, r^+) - 1; \tag{37}$$

$$Q(r^-, r^+) = \min \text{mod}(1, r^-, r^+); \tag{38}$$



$$Q(r^-, r^+) = \min \text{mod}[2, 2r^-, 2r^+, 0.5(r^- + r^+)];$$
(39)

$$Q(r^-, r^+) = \max\{0, \min(2r^-, 1), \min(r^-, 2)\} + \max\{0, \min(2r^+, 1), \min(r^+, 2)\} - 1;$$
(40)

$$Q(r^-, r^+) = \frac{r^- + |r^-|}{1 + r^-} + \frac{r^+ + |r^+|}{1 + r^+} - 1.$$
(41)

Normally the “minmod” function of two arguments is defined as

$$\min \text{mod}(x, y) = \text{sign}(x) \cdot \max\{0, \min[|x|, y \cdot \text{sign}(x)]\};$$
(42)

and the argument r is defined as:

$$r^- = \frac{\alpha_{i-1}^m}{\alpha_i^m} \quad \text{and} \quad r^+ = \frac{\alpha_{i+1}^m}{\alpha_i^m}$$
(43)

Finally, the dissipation operator at the interface “l” is defined as:

$$\{D_{Yee}\}_l = [R]_l \{\psi(\lambda_l)(1 - Q_l)\alpha_l\}$$
(44)

and the numerical flux vector is given by:

$$VF_l^{(m)} = (E_l^{(m)}h_x + F_l^{(m)}h_y + G_l^{(m)}h_z)\mathcal{V}_l - 0.5D_{Yee}^{(m)},$$
(45)

The time integration is performed by Eq. (21).

8. Yee and Harten (1987) TVD Algorithm

The symmetrical algorithm of [6], second order accurate in space, follows Eqs. (3) to (10). The next step is the determination of the g numerical speed of propagation of information:

$$g_i^m = S \cdot \max\{0, \min(|\lambda_l|, S \cdot \alpha_{i-1}^m)\}, \text{ where } : S = \text{sign}(\alpha_i^m).$$
(46)

The entropy function is defined by Eq. (12) and the numerical speed of information propagation is determined by:

$$\gamma_i^m = \frac{1}{2}\psi(\lambda_l) \cdot \begin{cases} (g_{i+1}^m - g_i^m)/\alpha^m, & \text{if } \alpha^m \neq 0.0 \\ 0.0, & \text{otherwise} \end{cases}$$
(47)

The numerical characteristic speed, ϕ , is expressed by:

$$\phi_m = \frac{1}{2}\psi(\lambda_l)(g_i + g_{i+1}) - \psi(\lambda_l + \gamma_i^m)\alpha^m$$
(48)

Finally, the dissipation function of [6], to second order of spatial accuracy, is constructed by the following matrix-vector product:

$$\{D_{Yee/Harten}\}_l = [R]_l \{\phi_m\}_l$$
(49)

and Eqs. (19), (20), (22) and (21) are used to determine the dissipation operator of the [6] scheme.

9. Hughson and Beran (1991) TVD Algorithm

The algorithm of [7], second order accurate in space, follows the Eqs. (3) to (10). The next step consists in determining the g numerical flux function. To non-linear fields (m = 1 and 5), it is possible to write:

$$g_i^m = \begin{cases} \frac{\alpha_i^m \alpha_{i-1}^m + |\alpha_i^m \alpha_{i-1}^m|}{\alpha_i^m + \alpha_{i-1}^m}, & \text{if } (\alpha_i^m + \alpha_{i-1}^m) \neq 0.0 \\ 0.0, & \text{if } (\alpha_i^m + \alpha_{i-1}^m) = 0.0 \end{cases}$$
(50)

To linear fields (m = 2, 3 and 4), it is possible to write:



$$g_i^m = \text{signal}_m \times \text{MAX}\left(0.0; \text{MIN}\left(\alpha_{i-1}^m, \alpha_i^m \times \text{signal}_m\right)\right), \tag{51}$$

Where signal_m assumes the value 1.0 if $\alpha_{i-1}^m \geq 0.0$ and -1.0 otherwise. After that, the Eqs. (11) and (12) are employed and the σ_m term is defined at the “I” interface as:

$$\sigma_m = 0.5(\psi_m - Z_m^2). \tag{52}$$

The ϕ_m numerical characteristic speed at the “I” interface is defined by:

$$\phi_m = \begin{cases} \sigma_m (g_{i+1}^m - g_i^m) / \alpha^m, & \text{if } \alpha^m \neq 0.0 \\ 0.0, & \text{if } \alpha^m = 0.0 \end{cases}. \tag{53}$$

The entropy function is redefined considering $\phi_m: Z_m = v_m + \phi_m$ and ψ_m is recalculated according to Eq. (12). Finally, the dissipation function of [7], to second order accurate in space, is constructed by the following matrix-vector product:

$$\{D_{\text{Hughson/Beran}}\}_I = [R]_I \left\{ \frac{[\sigma(g_i + g_{i+1}) - \psi \alpha]}{\Delta t_i} \right\}. \tag{54}$$

After that, Eqs. (19), (20) and (22) are used to conclude the numerical flux vector of the [7] scheme and Eq. (21) is employed to perform the time integration.

10. Harten and Osher (1987) TVD/ENO Algorithm

The numerical algorithm of [9], second order accurate in space, employs Eqs. (3-10). The next step consists in constructing the TVD/ENO numerical flux vector. Initially, it is necessary to define the σ parameter at the “I” interface to calculate the numerical velocity of information propagation, which contributes to the second order spatial accuracy of the scheme:

$$\sigma(z) = 0.5[\Psi(z) - \Delta t_i z^2]; \tag{55}$$

with $\Psi(z)$ defined according to Eq. (12) and z defined as the eigenvalues at the interface, Eq. (7). The non-linear limited flux function, based on the idea of a modified flux function of [2], is constructed by:

$$\bar{\beta}_i^m = m[\alpha_i^m - \zeta \bar{m}(\Delta_+ \alpha_i^m, \Delta_- \alpha_i^m), \alpha_{i-1}^m + \zeta \bar{m}(\Delta_+ \alpha_{i-1}^m, \Delta_- \alpha_{i-1}^m)], \tag{56}$$

where the m and \bar{m} limiters are defined as:

$$m(y, z) = \begin{cases} s \times \text{MIN}(|y|, |z|), & \text{if } \text{signal}(y) = \text{signal}(z) = s \\ 0, & \text{otherwise} \end{cases}; \tag{57}$$

$$\bar{m}(y, z) = \begin{cases} y, & \text{if } |y| \leq |z| \\ z, & \text{if } |y| > |z| \end{cases}; \tag{58}$$

and the forward and backward operators are defined according to:

$$\Delta_+ = (\cdot)_{i+1} - (\cdot)_i \text{ and } \Delta_- = (\cdot)_i - (\cdot)_{i-1}. \tag{59}$$

The numerical velocity of information propagation is calculated by:

$$\bar{\gamma}_i^m = \sigma(\lambda_i^m) \begin{cases} (\bar{\beta}_{i+1}^m - \bar{\beta}_i^m) / \alpha^m, & \text{if } \alpha^m \neq 0; \\ 0, & \text{otherwise.} \end{cases} \tag{60}$$

The dissipation function to the TVD and ENO versions of the [9] scheme is defined as:

$$(\phi_i^m)_{\text{HO}} = \sigma(\lambda_i^m) (\bar{\beta}_i^m + \bar{\beta}_{i+1}^m) - \Psi(\lambda_i^m + \bar{\gamma}_i^m) \alpha_i^m, \tag{61}$$

with: “I” assuming values from 1 to 5 (three-dimensional space), ϵ assuming the value 0.2 recommended by [9], Ψ is the entropy function to guarantee that only relevant physical solutions are admissible, and ζ assumes the

value 0.0 to obtain the TVD scheme of [2], second order accurate, and 0.5 to obtain the essentially non-oscillatory scheme, uniform second order accuracy in the field, of [9].

Finally, the dissipation operator of [9], to second order of spatial accuracy, in its TVD and ENO versions, is constructed by the following matrix-vector product:

$$\{D_{\text{Harten / Osher}}\}_1 = [R]_1 \{\phi_{\text{HO}}\}_1 \tag{62}$$

The complete numerical flux vector to the “1” interface is described by Eqs. (19), (20), and (22) whereas the time integration is performed by the Runge-Kutta method of Eq. (21).

11. Yang (1991) TVD/ENO Algorithm

11.1. Yang TVD of third order

According to [17], a conservative scheme for Eq. (1) can be expressed as:

$$Q_i^{n+1} = Q_i^n - \lambda (VF_1^N + VF_2^N + VF_3^N + VF_4^N) \tag{63}$$

and the numerical flux VF_1^N , for example, is given by:

$$VF_1^N = F_{i+1}^M - \hat{A}_1^+ \Delta_+ F_i^M = F_i^M + \hat{A}_1^- \Delta_+ F_i^M \tag{64}$$

A third order scheme for Eq. (1) can be expressed in terms numerical flux of the form Eq. (64) with:

$$F_i^M = F_i^{\text{TVD}3} = F_i^n + D_i^n \tag{65}$$

The components of D_i are given by

$$d_i^m = [1 - S(\theta_i^m)] \tilde{d}_i^m + [1 + S(\theta_i^m)] \bar{d}_{i-1}^m \tag{66}$$

where \tilde{d}_i^m and \bar{d}_{i-1}^m are components of \tilde{D}_i and \bar{D}_i given, respectively, by

$$\tilde{D}_i = \text{sign}(A_1) (\lambda^2 |A_1|^2 - 3\lambda |A_1| + 2I) \Delta_+ F_i / 6 \tag{67}$$

and $S(\theta_i^m)$ is the smoothness monitor given by [23] as

$$S(\theta_i^m) = 0, \quad \text{if } |\Delta_+ q_i^m| + |\Delta_- q_i^m| = 0 \quad \text{or} \quad S(\theta_i^m) = \frac{|\Delta_+ q_i^m| - |\Delta_- q_i^m|}{|\Delta_+ q_i^m| + |\Delta_- q_i^m|}, \quad \text{otherwise} \tag{68}$$

where q_i^m are components of the conservative state vector Q_i .

11.2. Yang ENO third order

Unlike TVD schemes, nonoscillatory schemes are not required to damp the values of each local extremum at every single time step but are allowed to occasionally accentuate a local extremum.

The design involves an essentially non oscillatory piecwork polynomial reconstruction of the solution from its cell averages, time evolution through an approximate solution of the resulting initial value problem, and averaging of this approximate solution over each cell.

A third order ENO scheme for Eq. (1) can be constructed using Reconstruction via Primitive variable and $N = 3$. Here

$$F_i^M = F_i^{\text{ENO}3} = F_i^n + E_i^n + D_i^n \tag{69}$$

and E and D are terms that make up for the higher order accuracy that also demands either the TVD or the ENO property to avoid Gibbs phenomena.

In Equation (69) the components of the column vector E_i are given by

$$e_i^m = m(\tilde{e}_i^m, \tilde{e}_{i-1}^m) \tag{70}$$

Where m is defined by Eq. (57) and the terms \tilde{e}_i^m are given by

$$\tilde{E}_i = \text{sign}(A_1) (I - \lambda |A_1|) \Delta_+ F_i / 2 \tag{71}$$

and the components of column vector D_j are given by

$$d_i^m = m(\Delta_- \tilde{d}_{i-1}^m, \Delta_+ \tilde{d}_{i-1}^m) \quad \text{if} \quad |\Delta_- q^m| \leq |\Delta_+ q^m| \quad \text{or} \quad d_i^m = m(\Delta_- \hat{d}_i^m, \Delta_+ \hat{d}_i^m) \quad \text{if} \quad |\Delta_- q^m| > |\Delta_+ q^m|, \quad (72)$$

where \tilde{d}_i^m and \hat{d}_i^m are components of \tilde{D}_i and \hat{D}_i , respectively. \tilde{D}_i is given by Eq. (67) and \hat{D}_i is given by

$$\hat{D}_i = \text{sign}(A_1)(\lambda^2 |A_1|^2 - I) \Delta_+ F_i / 6. \quad (73)$$

The first author introduced a modification, changing the difference in terms of the flux vector, Eqs. (67) and (73), by the difference in terms of the conserved variable vector. With it, the matrix A is modified in order to take into account this operation. Details of the modification in the matrix A can be seen in [24]. With such modification the algorithm captures shock wave more clearly and accurately.

12. Yang and Hsu (1992) UNO Algorithm

The UNO scheme of [18] is equivalent to an ENO scheme of third order of accuracy. The components of $\varphi_i^{\text{UNO}3}$ are defined as:

$$\varphi_i^{\text{UNO}3} = \sigma(\lambda_i^m)(\beta_i^m + \beta_{i+1}^m) + \begin{cases} \bar{\sigma}(\lambda_i^m)(\bar{\beta}_i^m + \bar{\beta}_{i+1}^m) - \psi(\lambda_i^m + \gamma_i^m + \bar{\gamma}_i^m)\alpha_i^m, & \text{if } |\alpha_{i-1}^m| \leq |\alpha_i^m| \\ \hat{\sigma}(\lambda_i^m)(\hat{\beta}_i^m + \hat{\beta}_{i+1}^m) - \psi(\lambda_i^m + \gamma_i^m + \hat{\gamma}_i^m)\alpha_i^m, & \text{if otherwise} \end{cases}; \quad (74)$$

where the σ , $\bar{\sigma}$, and $\hat{\sigma}$ functions are given by:

$$\sigma = \frac{1}{2}[\psi(z) - \lambda z^2]; \quad \bar{\sigma} = \frac{1}{6}[2|z| - 3\lambda|z|^2 + \lambda^2|z|^3]; \quad \text{and} \quad \hat{\sigma} = \frac{1}{6}[\lambda^2|z|^3 - |z|]. \quad (75)$$

The β , $\bar{\beta}$, and $\hat{\beta}$ are parameters defined by:

$$\beta = m[\alpha_i^m, \alpha_{i-1}^m]; \quad (76)$$

$$\bar{\beta} = \bar{m}[\Delta_- \alpha_{i-1}^m, \Delta_+ \alpha_{i-1}^m] \quad \text{if} \quad |\alpha_{i-1}^m| \leq |\alpha_i^m|; \quad (77)$$

$$\hat{\beta} = \bar{m}[\Delta_- \alpha_i^m, \Delta_+ \alpha_i^m] \quad \text{if} \quad |\alpha_{i-1}^m| > |\alpha_i^m|. \quad (78)$$

and finally, the γ , $\bar{\gamma}$, and $\hat{\gamma}$ numerical speed of propagation of information are given by:

$$\gamma = \sigma(\lambda_i^m) \begin{cases} (\beta_{i+1}^m - \beta_i^m) / \alpha_i^m & \text{if } |\alpha_i^m| \neq 0.0; \\ 0.0 & \text{otherwise} \end{cases}; \quad (79)$$

$$\bar{\gamma} = \bar{\sigma}(\lambda_i^m) \begin{cases} (\bar{\beta}_{i+1}^m - \bar{\beta}_i^m) / \alpha_i^m & \text{if } |\alpha_i^m| \neq 0.0; \\ 0.0 & \text{otherwise} \end{cases}; \quad (80)$$

$$\hat{\gamma} = \hat{\sigma}(\lambda_i^m) \begin{cases} (\hat{\beta}_{i+1}^m - \hat{\beta}_i^m) / \alpha_i^m & \text{if } |\alpha_i^m| \neq 0.0; \\ 0.0 & \text{otherwise} \end{cases}; \quad (81)$$

Finally, the dissipation operator of [18], to third order of spatial accuracy, in its UNO version, is constructed by the following matrix-vector product:

$$\{D_{\text{Yang/Hsu}}\}_1 = [R]_1 \{\varphi^{\text{UNO}3}\}_1. \quad (82)$$

The complete numerical flux vector to the “1” interface is described by Eqs. (19), (20), and (22) whereas the time integration is performed by the Runge-Kutta method of Eq. (21).

13. Spatially Variable Time Step

The basic idea of this procedure consists in keeping constant the CFL number in all calculation domain, allowing, hence, the use of appropriated time steps to each specific mesh region during the convergence process. According to the definition of the CFL number, it is possible to write:



$$\Delta t_i = \text{CFL}(\Delta s)_i / c_i, \quad (83)$$

where CFL is the ‘‘Courant-Friedrichs-Lewy’’ number to provide numerical stability to the scheme; $c_i = \left[\sqrt{u^2 + v^2 + w^2} + a \right]_i$ is the maximum characteristic speed of propagation of information in the calculation domain; and $(\Delta s)_i$ is a characteristic length of transport of information. On a finite volume context, $(\Delta s)_i$ is chosen as the value found to the minimum cell side length.

14. Physical Problems

The first problem to be studied is the transonic convergent-divergent nozzle. The geometry of the convergent-divergent nozzle at the xy plane is described in Fig. 1. The total length of the nozzle is 0.38ft (0.116m) and the throat height is equal to 0.090ft (0.027m). The throat is located at 0.19ft (0.058m) from the entrance boundary. The throat curvature ratio is equal to 0.090ft. The nozzle convergence angle is 22.33° and the nozzle divergence angle is 1.21° . An exponential stretching of 10% in both normal and tangent lines was used. An algebraic mesh of 61 points in the tangent direction, 71 points in the normal direction, and 10 points in the span direction was generated, which corresponds in finite volumes to 226,800 tetrahedral cells and 43,310 nodes. Figure 2 exhibits the mesh employed in the simulations.

The second problem is the ramp problem. The ramp configuration at the xy plane is described in Fig. 3. The compression corner has 20° of inclination. The mesh used in the simulations has 158,760 rectangular cells and 30,500 nodes to a structured discretization of the calculation domain. This mesh is equivalent, in finite differences, of being composed of 61 points in the tangent direction, 50 points in the normal direction, and 10 points in the span direction. Figure 4 shows such mesh. The initial and boundary conditions are described in [21].

The employed meshes were the best where convergence was obtained by the numerical schemes.

Therefore, grid independence study was not performed. The differences in the solutions are due to the algorithm performance and are characteristic of each scheme.

In the present work, it is adopted the following nomenclature for the results:

YWH82 – It refers to the Yee, Warming and Harten (1982) scheme, [1];

H83 – It refers to the Harten (1983) scheme, [2];

YWH85 – It refers to the Yee, Warming and Harten (1985) scheme, [4];

YH87 – It refers to the Yee and Harten (1987) scheme, [6];

HB91 – It refers to the Hughson and Beran (1991) scheme, [7].

Only the YWH82, H83, YWH85, YH87, and HB91 schemes have presented converged solutions. The YH87 scheme did not present converged results for the nozzle problem, whereas the YWH85 scheme did not present converged results for the ramp problem.

15. Results

15.1. Nozzle problem

Figures 5 and 6 present the pressure and Mach number contours, respectively, predicted using the YWH82 scheme. Both pressure and Mach number contours present bad quality. The weak shock wave at the nozzle throat is well captured by the YWH82 scheme.

Figures 7 to 12 present similar results for the H83, YWH85 and HB91 schemes. The shock wave at the nozzle throat is accurately well captured by these schemes.

Finally, Figure 13 shows the wall pressure ratio calculated by the four schemes. The pressure distributions are compared with the experimental results of [25]. The best wall pressure distribution is due to H83.

15.2. Ramp problem

For this problem, a supersonic Mach number of 2.0 and the entrance and longitudinal angles of 0.0° were employed as initial condition.



Figures 14 and 15 exhibit the pressure and Mach number contours obtained by the YWH82 scheme. The shock wave and the expansion fan are appropriately captured by the numerical algorithm. The curves of contours are of reasonable quality.

Figures 16 to 21 show the pressure and Mach number contours calculated by the H83, YH87 and HB91 schemes, respectively. All solutions present good contours of pressure and of Mach number; However, the YH87 presents the best distributions in relation to the other schemes. The Mach number fields are free of pre-shock oscillations in all solutions.

Figures 22 shows the wall pressure distributions obtained with the TVD schemes. They are compared with the shock wave and expansion fan relations of [26]. The best distribution is due to the YH87 scheme, numerical plateau closer to the theoretical plateau.

A way to quantitatively verify if the solutions generated by each scheme are satisfactory consists in determining the shock angle of the oblique shock wave, β , measured in relation to the initial direction of the flowfield. [26] presents a diagram with values of the shock angle, β , to oblique shock waves. The value of this angle is determined as function of the freestream Mach number and of the deflection angle of the flow after the shock wave, ϕ . To $\phi = 20^\circ$ (ramp inclination angle) and to a freestream Mach number equals to 2.0, it is possible to obtain from this diagram a value to β equals to 53.0° . Using a transfer in all pressure contours figures, it is possible to obtain the values of β to each scheme, as well the respective errors, shown in Tab. 1. As can be noted, the best result is due to YH87 with an error of 5.66%. Hence, in this supersonic problem, the YH87 was the best. The other results have presented errors for β very high due to the capacity of each algorithm to capture the shock wave appropriately. The YH87 scheme was the unique sufficient capable to capture these properties.

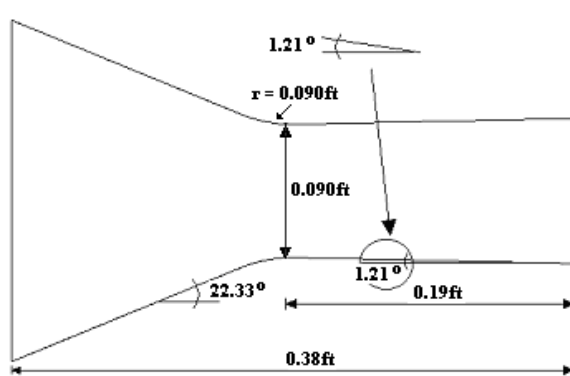


Figure 1: Nozzle configuration

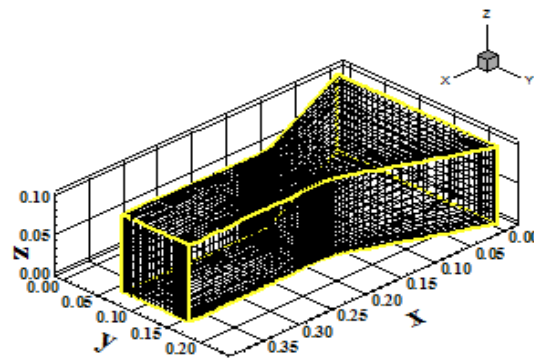


Figure 2: Structured nozzle mesh

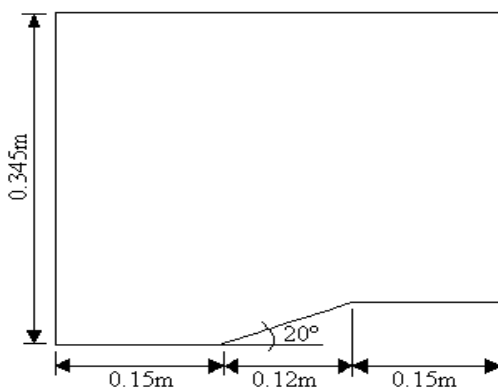


Figure 3: Ramp configuration

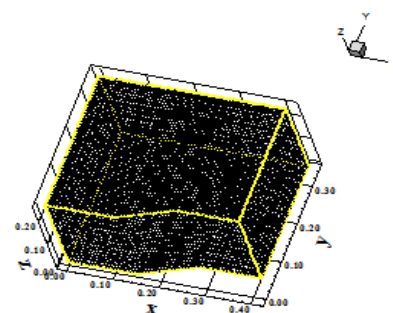


Figure 4: Structured ramp mesh

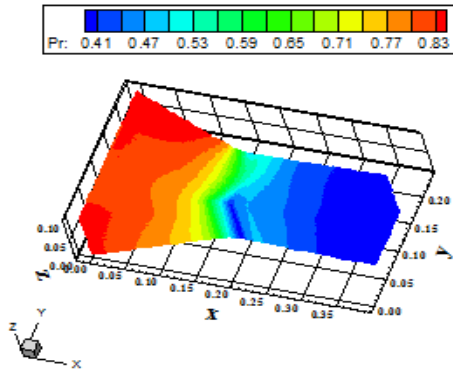


Figure 5: Pressure contours (YWH82)

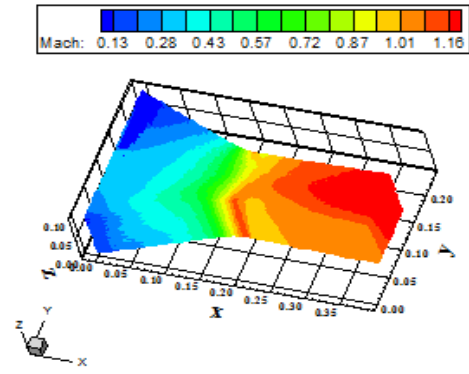


Figure 6: Mach number contours (YWH82)

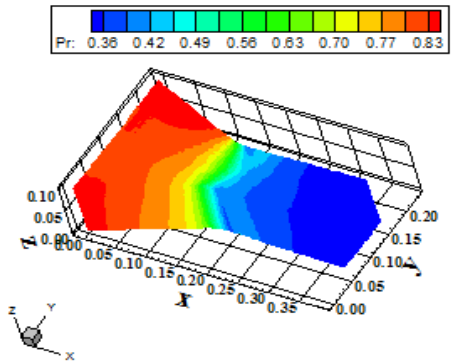


Figure 7: Pressure contours (H83)

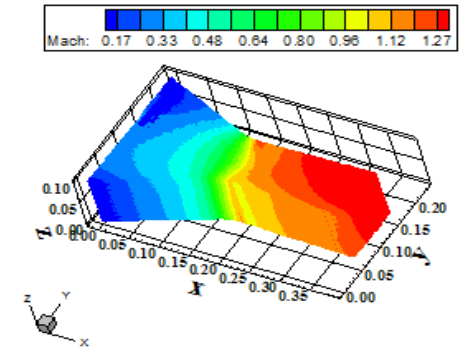


Figure 8: Mach number contours (H83)

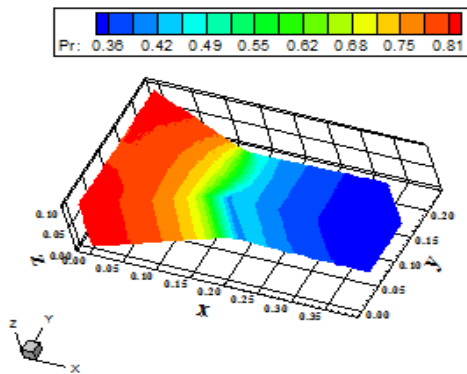


Figure 9: Pressure contours (YWH85)

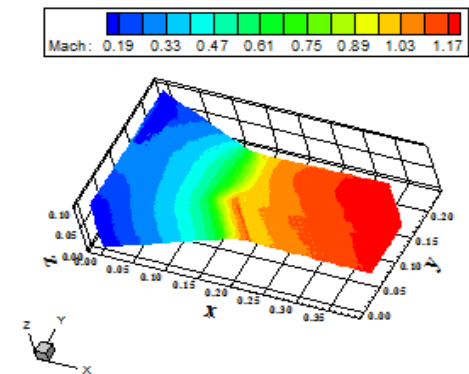


Figure 10: Mach number contours (YWH85)

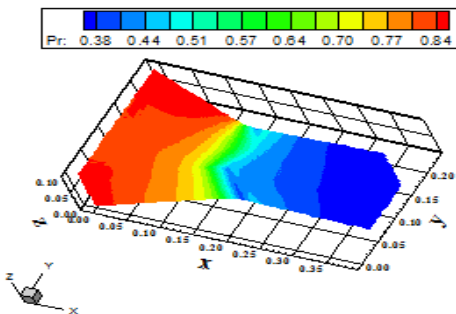


Figure 11: Pressure contours (HB91)

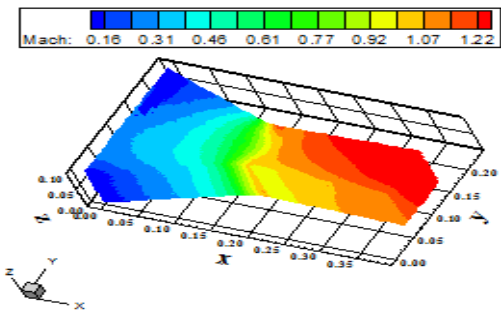


Figure 12: Mach number contours (HB91)

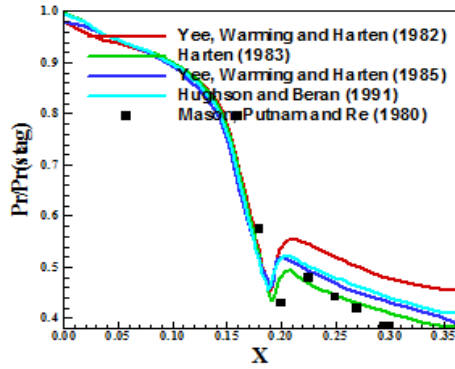


Figure 13: Wall pressure distribution at wall

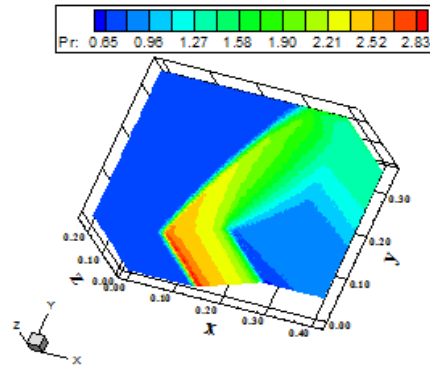


Figure 14: Pressure contours (YWH82)

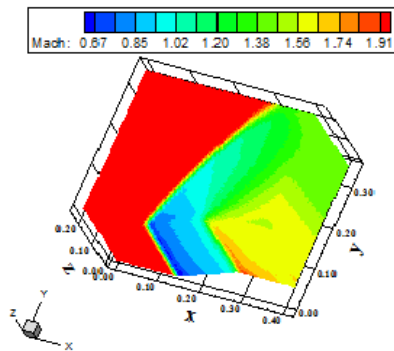


Figure 15: Mach number contours (YWH82)

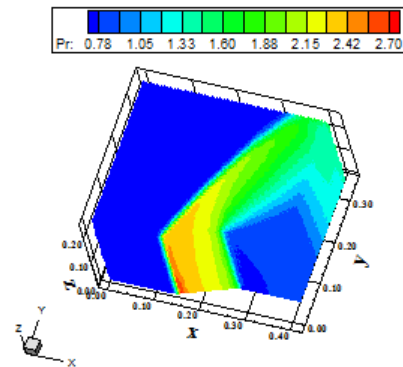


Figure 16: Pressure contours (H83)

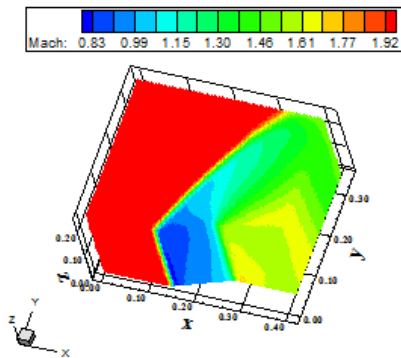


Figure 17: Mach number contours (H83)

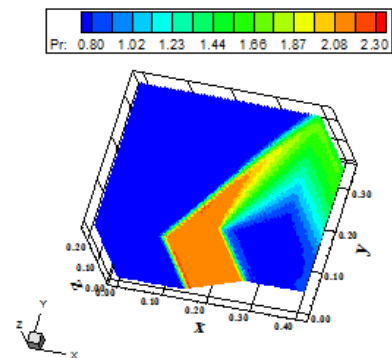


Figure 18: Pressure contours (YH87)

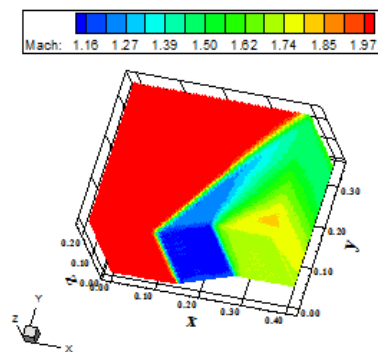


Figure 19: Mach number contours (YH87)

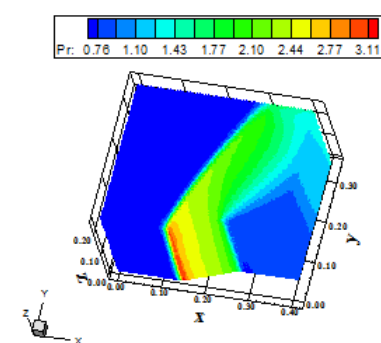


Figure 20: Pressure contours (HB91)

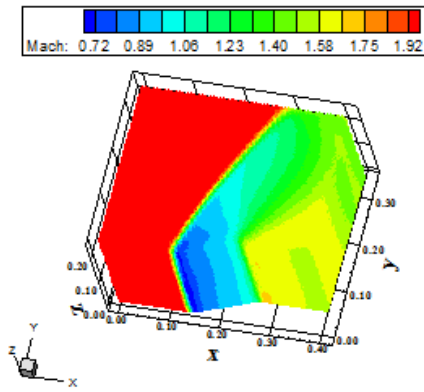


Figure 21: Mach number contours (HB91)

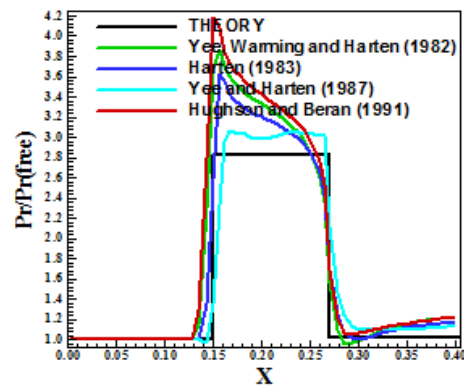


Figure 22: Wall pressure distribution at wall

Table 1: Comparison among shock wave angles and respective errors

Scheme	β (°)	Error (%)
YWH82	70.0	32.07
H83	67.0	26.42
YH87	56.0	5.66
HB91	72.0	35.85

16. Conclusions

In this paper, the Euler equations in three-dimensions were solved by the use of TVD, ENO and UNO schemes, second and third order accurate. The following ten flux difference splitting algorithms were employed: [1-7], on a TVD approach and [9, 17], on an ENO approach, and finally [18], on an UNO approach. A finite volume formulation was employed on conservative and unstructured contexts. The time discretization employed a Runge-Kutta method of two steps. All ten algorithms were applied to the solution of two problems: the transonic convergent-divergent symmetrical nozzle, and the supersonic ramp. All schemes were accelerated to the steady state solution using a spatially variable time step procedure, which had proved excellent characteristics of convergence [19-20]. The results have demonstrated that the best result of the wall pressure distribution in the nozzle case was due to [2] and the best wall pressure distribution and shock angle in the ramp case was due to [6].

The main contribution of this study was to highlight the [2] scheme as able to capture the main aspects of the flowfield as well the best wall pressure distribution in the nozzle case and the [6] scheme as able to capture the main aspects of the flowfield and the best shock wave angle with accuracy (error less than 6.00%). Moreover, the implementation of these schemes on an unstructured context is also a significant and important contribution to the CFD community.

Acknowledgments

The first author would like to thank CAPES by the scholarship which permitted the accomplishment of this work. He also thanks the ITA by the infra-structure that also allowed the realization of this work.

References

- [1]. H. C. Yee, R. F. Warming, and A. Harten, “A High-Resolution Numerical Technique for Inviscid Gas-Dynamic Problems with Weak Solutions”, Proceedings of the 8th International Conference on Numerical Methods in Fluid Dynamics, E. Krause, Editor, *Lecture Notes in Physics*, Vol. 170, 1982, pp. 546-552, Springer-Verlag, Berlin, Germany.
- [2]. A. Harten, “High Resolution Schemes for Hyperbolic Conservation Laws”, *Journal of Computational Physics*, Vol. 49, No. 2, 1983, pp. 357-393.



- [3]. H. C. Yee, and P. Kutler, “Application of Second-Order-Accurate Total Variation Diminishing (TVD) Schemes to the Euler Equations in General Coordinates”, *NASA-TM-85845*, 1985.
- [4]. H. C. Yee, R. F. Warming, and A. Harten, Implicit Total Variation Diminishing (TVD) Schemes for Steady-State Calculations, *Journal of Computational Physics*, Vol. 57, No. 3, 1985, pp. 327-360.
- [5]. H. C. Yee, “Construction of Explicit and Implicit Symmetric TVD Schemes and Their Applications”, *Journal of Computational Physics*, Vol. 68, 1987, pp. 151-179.
- [6]. H. C. Yee, and A. Harten, “Implicit TVD Schemes for Hyperbolic Conservation Laws in Curvilinear Coordinates”, *AIAA Journal*, Vol. 25, No. 2, 1987, pp. 266-274.
- [7]. M. C. Hughson, and P. S. Beran, “Analysis of Hyperbolic Blunt-Body Flows Using a Total Variations Diminishing (TVD) Scheme and the MacCormack Scheme”, *AIAA 91-3206-CP*.
- [8]. H. C. Yee, “A Class of High-Resolution Explicit and Implicit Shock-Capturing Methods”, *NASA TM-101088*, 1989.
- [9]. A. Harten, and S. Osher, Uniformly High Order Accurate Non-Oscillatory Schemes, *SIAM J. Num. Anal.*, Vol. 24, No. 2, 1987, pp. 279-309.
- [10]. A. Harten, B. Engquist, S. Osher, and S. R. Chakravarthy, Uniformly High Order Accurate Essentially Non-Oscillatory Schemes. II., Preprint, 1986.
- [11]. A. Harten, B. Engquist, S. Osher, and S. R. Chakravarthy, Some Results on Uniformly High Order Accurate Essentially Non-Oscillatory Schemes, *Advances in Numerical Analysis and Applied Mathematics*, edited by J. C. South, Jr. and M. Y. Hussaini, *ICASE Rept. 86-18*; also *Journal of Applied Num. Mathematics*, Vol. 2, 1986, pp. 347-367.
- [12]. A. Harten, B. Engquist, S. Osher, and S. R. Chakravarthy, Uniformly High Order Accurate Essentially Non-Oscillatory Schemes. III., *ICASE Rept. 86-22*, 1986.
- [13]. S. K. Godunov, “A Difference Scheme for Numerical Computation of Discontinuous Solution of Hydrodynamic Equations”, *Math. Sbornik*, Vol. 47, 1958, pp. 271-306.
- [14]. P. Colella, and P. R. Woodward, “The Piecewise-Parabolic Method (PPM) for Gas-Dynamics Simulation”, *Journal of Computational Physics*, Vol. 54, No. 1, 1984, pp. 174-201.
- [15]. B. Van Leer, “Towards the Ultimate Conservative Difference Scheme. V. A Second Order Sequel to Godunov’s Method”, *Journal of Computational Physics*, Vol. 32, 1979, pp. 101-136.
- [16]. S. Osher, and S. R. Chakravarthy, “High Resolution Schemes and Entropy Conditions”, *SIAM Journal of Numerical Analysis*, Vol. 21, No. 4, 1984, pp. 955-984.
- [17]. J. Y. Yang, “Third-Order Nonoscillatory Schemes for the Euler Equations”, *AIAA Journal*, Vol. 29, No. 10, 1991, pp. 1611-1618.
- [18]. J. Y. Yang, and C. A. Hsu, “High-Resolution, Nonoscillatory Schemes for Unsteady Compressible Flows”, *AIAA Journal*, Vol. 30, No. 6, 1992, pp. 1570-1575.
- [19]. E. S. G. Maciel, *Simulations in 2D and 3D Applying Unstructured Algorithms, Euler and Navier-Stokes Equations – Perfect Gas Formulation*. Saarbrücken, Deutschland: Lambert Academic Publishing (LAP), 2015, Ch. 1, pp. 26-47.
- [20]. E. S. G. Maciel, *Simulations in 2D and 3D Applying Unstructured Algorithms, Euler and Navier-Stokes Equations – Perfect Gas Formulation*. Saarbrücken, Deutschland: Lambert Academic Publishing (LAP), 2015, Ch. 6, pp. 160-181.
- [21]. E. S. G. Maciel, and E. M Ferreira, *Applications of TVD and ENO Algorithms in 2D and 3D, Euler and Navier-Stokes Equations*. Saarbrücken, Deutschland: Lambert Academic Publishing (LAP), 2015.
- [22]. E. S. G. Maciel, “Explicit and Implicit TVD and ENO High Resolution Algorithms Applied to the Euler and Navier-Stokes Equations in Three-Dimensions – Theory”, *Proceedings of the 20th International Congress of Mechanical Engineering (XX COBEM)*, Gramado, RS, Brazil. [CD-ROM]
- [23]. B. Van Leer, “Towards the Ultimate Conservative Difference Scheme II, Monotonicity and Conservation Combined in a Second Order Scheme”, *Journal of Computational Physics*, Vol. 14, 1974, pp. 361-370.



- [24]. E. S. G. Maciel, and C. R. Andrade, “Comparison Among Unstructured TVD, ENO and UNO Schemes in Two-Dimensions”, *Journal of Advances in Mathematics and Computer Science*, Vol. 25, Issue 1, 2017, pp. 1-31.
- [25]. M. L. Mason, L. E. Putnam, and R. J. Re, “The Effect of Throat Contouring on Two-Dimensional Converging-Diverging Nozzles at Sonic Conditions”, *NASA Technical Paper 1704*, 1980.
- [26]. J. D. Anderson Jr., *Fundamentals of Aerodynamics*, McGraw-Hill, Inc., 5th Edition, 1008p., 2010.

